Journal of Nuclear Materials 573 (2023) 154122

Contents lists available at ScienceDirect

Journal of Nuclear Materials

journal homepage: www.elsevier.com/locate/jnucmat

Determination of the hydrogen heat of transport in Zircaloy-4

Soyoung Kang[a,*], Pei-Hsun Huang[b], Victor Petrov[b,c,d], Annalisa Manera[b,c,d], Taehwan Ahn[b], Bruce Kammenzind[e], Arthur T. Motta[a]

[a] Ken and Mary Alice Lindquist Department of Nuclear Engineering, The Pennsylvania State University, University Park, PA 16802, USA
[b] Department of Nuclear Engineering & Radiological Sciences, University of Michigan – Ann Arbor, 2355 Bonisteel Blvd, Ann Arbor, MI 48109, USA
[c] ETH Zürich, Department of Mechanical and Process Engineering, Sonneggstrasse 3, 8092 Zürich, Switzerland
[d] Laboratory for Reactor Physics and Thermal-Hydraulics (LRT), Paul Scherrer Institute, 5232 Villigen PSI, Switzerland
[e] Fluor Marine Propulsion, Bettis Laboratory, PO Box 79, West Mifflin, PA 15122, USA

ARTICLE INFO

Article history:
Received 1 August 2022
Revised 21 October 2022
Accepted 2 November 2022
Available online 3 November 2022

Keywords:
Heat of transport
Zircaloy
Hydrogen migration
Hydrogen distribution
Bison

ABSTRACT

During operation in a nuclear reactor, Zr-based nuclear fuel cladding is subject to waterside corrosion which can lead to hydrogen ingress. The hydrogen that enters the material will migrate to colder spots and precipitate as zirconium hydrides if the hydrogen content exceeds the hydrogen terminal solid solubility in the material. Since a temperature gradient is established in the radial direction of the cladding during operation, the hydrides can preferentially precipitate at the colder outer surface of the cladding. Other gradients can also occur in the longitudinal and azimuthal directions of the cladding tube. As a consequence, hydrogen redistributes itself in response to the concentration and temperature gradients present in the sample. The response of the hydrogen in solid solution to temperature gradients is governed by the heat of transport Q^* as a function of temperature, so it can be used in the BISON code. A set of experiments was set up to determine the heat of transport (Q^*), in which a uniformly hydrided Zircaloy-4 sample is annealed under a fixed temperature gradient at a range of temperatures, and the resulting hydrogen distribution is analyzed to determine Q^*. The results are discussed in terms of existing literature.

1. Introduction

Zirconium alloys have been extensively used for nuclear reactor fuel cladding [1]. During normal reactor operation, the zirconium alloy cladding is in contact with the reactor coolant water and corrodes by the oxidation reaction expressed by Eq. (1)

$$Zr + 2H_2O \rightarrow ZrO_2 + 2H_2 \quad (1)$$

The oxidation reaction between the cladding and the cooling water releases hydrogen from the water, and some of this hydrogen is picked up into the Zr-based nuclear fuel cladding [2]. We note that the hydrogen entering the cladding is thought to be due to corrosion rather than to additional dissolved hydrogen from radiolysis or hydrogen water chemistry [3]. The hydrogen remains in solid solution in the Zr matrix during operation until its concentration reaches the terminal solid solubility (TSS) at operating temperature at which point it is then precipitated as zirconium hydrides. Because these hydrides are more brittle than the Zr matrix, hydride-induced embrittlement can be an important contributor to the possible degradation of cladding ductility [4].

The distribution of hydrides in irradiated fuel rods is not homogeneous, but varies depending on the gradients of temperature and solid solution hydrogen concentration present during normal operation and dry storage. This causes the hydrides to be unevenly distributed within the cladding. Specifically, the hydrides are preferentially accumulated at the cold spots in the cladding, and because the outer part of the cladding tube is coldest, they can form a dense hydride layer or “hydride rim” near the outer diameter [4]. The fracture strains for the cladding tube decrease with hydride rim thickness thus degrading cladding ductility. Therefore, it is important to develop a tool that can predict hydrogen migration and redistribution and implement it into the fuel performance code BISON to be able to effectively predict hydrogen induced degradation of cladding performance through life.

When hydrogen is in solid solution in a zirconium alloy its migration is driven both by a solid solution hydrogen concentration gradient (Fick’s Law) and by a temperature gradient (Soret Effect) [5,6]. The hydrogen flux from these two effects is given by

* Corresponding author.
E-mail address: szk417@psu.edu (S. Kang).

https://doi.org/10.1016/j.jnucmat.2022.154122
0022-3115/

Eqs. (2) [7]:

$$J_H = -D_H \nabla C_H^{ss} - \frac{D_H C_H^{SS} Q^*}{RT^2} \nabla T \quad (2)$$

where T is the temperature, J_H is hydrogen flux; D_H is the hydrogen diffusion coefficient in the material; C_H^{ss} is the hydrogen concentration in solid solution; R is the gas constant and Q^* is the heat of transport. Note that this formulation neglects the effect of a stress field on the hydrogen flux [8]. This approximation is valid as long as large stress concentrators, (such as can occur near a crack tip or notch), are not present.

To use Eq. (2), it is necessary to obtain accurate values of the heat of transport (Q^*), as it governs the Soret effect. Q^* is assumed to have a constant value of 25,070 J/mol in the BISON fuel performance code. A close analysis of Kammenzind's experiments [9] as reviewed by Merlino [10] casts some doubt on this conclusion. Therefore, this paper presents an experiment designed to determine the heat of transport (Q^*) so that the existing hydrogen migration predictions in BISON can be made more accurate. This is described in the following Section 4 (discussion).

2. Experimental methods

The experiment consists of gas charging a Zircaloy-4 sheet sample uniformly with hydrogen and subjecting it to a long anneal (on the order of a month) under a fixed linear temperature profile. Because of the Soret effect, the hydrogen migrates towards the colder part of the sample. At the end of the prescribed time, the sample is sectioned and the hydrogen profile resulting from the Soret effect redistribution of hydrogen is measured. From those measurements, the heat of transport can be evaluated.

Several runs of the experiment were conducted at a range of temperatures (varying both the high and the low temperatures). The experiment was designed to establish a high enough gradient to distribute the hydrogen during the anneal time and to run it long enough to reach a steady state. The temperature was tightly controlled during the experiment and did not vary by more than 3 °C at either end. The measurements of hydrogen content both before and after the experiment were conducted by hot vacuum extraction.

2.1. Hydrogen gas charging

Zircaloy -4 sheet in the cold worked stress relieved (CWSR) state was provided by ATI Specialty Alloys and Components. Its dimensions were 1.5 cm width x 6.5 cm length x 0.06 cm thickness. Before hydrogen charging the specimen, the Zircaloy-4 samples were etched in a solution of nitric acid (HNO_3): water (H_2O): hydrofluoric acid (HF) = 45 : 45 : 10 in vol. % to remove the native oxide layer that forms during exposure to air, and which can block hydrogen ingress. After etching, the Zircaloy-4 samples were quickly coated with a thin layer of nickel ($\approx$ 20 nm) using sputter deposition. This was done to prevent a reformation of the native oxide while still allowing hydrogen ingress during charging.

The coated Zircaloy-4 samples were hydrided using a gaseous hydrogen charging method. Fig. 1 shows the gaseous hydrogen charging machine used for that procedure. It consists of a furnace, a hydrogen container, and a quartz tube evacuated by rough and turbopumps. A hydrogen container gauge measured the hydrogen pressure in the container so that a specified amount of hydrogen can be introduced into the quartz tube. The rough and turbo pumps evacuated the quartz tube to a pressure of $< 10^{-6}$ Torr. After that, the chamber was heated to 400 °C, and a hydrogen and argon gas mixture (12.5% H_2 and 87.5% Ar) was released into the quartz tube, and the sample was annealed for 24 h. By following the pressure drop it was determined that hydrogen in the container entered the sample. Then the samples were furnace cooled at a rate of 1 °C/min. The hydrogen content in the samples was aimed for 200 wt.ppm so as not to exceed Terminal Solid Solubility for dissolution (TSS_d) at the planned test temperatures, and thus have all the hydrogen in solid solution throughout the experiment.

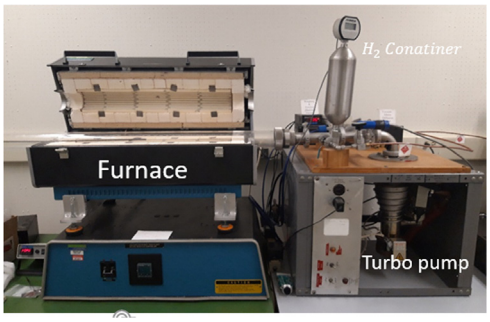

Fig. 1. Gaseous hydrogen charging apparatus.

2.2. Post charging analysis

After gaseous hydrogen charging, the nickel on the surface of the samples was mechanically removed using silicon carbide paper. The hydrided sheets (1.5 cm x 6.5 cm) were then cut into 1 cm x 4 cm samples in Fig. 2 and were used for the hydrogen migration experiments, conducted at the University of Michigan. The remaining area with the left and right sides of the samples was removed because it touched the sample holder. Three pieces from the bottom of the sample were used for the analysis of the initial hydrogen content (Fig. 2). In some experiments, the average of the three pieces on the bottom of the samples was used for determining initial hydrogen content. In other experiments, the average of the hydrogen content in three pieces on the bottom and the top of the samples was used. The hydrogen content among the different pieces varied within a range of 4-40 wt.ppm, suggesting some variation in charging content although this was not achieved in every case.

2.3. Sample anneal for hydrogen migration

Table 1 shows the tests conducted in this study. The temperature ranges were chosen so that calculations predicted a measurable result in a reasonable time. The annealing time for the hydrogen content to reach steady-state was determined by running the mHNGD model [5,11] using the initial hydrogen concentration and the expected temperature profile of each sample. In the initial tests by performing hydrogen measurements before and after the tests we found that the average hydrogen content in the samples increased during the tests. To mitigate this issue, in subsequent experiments the nickel on the surface of the samples was removed, and the samples were exposed to air to form a thin oxide layer to prevent hydrogen ingress during the experiment. This was done for all experiments listed in Table 1 except UM9, and it did help reduce the hydrogen ingress during the experiment.

We note, however, that whether or not hydrogen comes into the sample during the experiments would not affect the calculation of the heat of transport as long as: (i) the hydrogen that enters the sample has enough time to move in response to the temperature gradient established (which it is estimated to have at the temperatures of the tests) and (ii) that the overall hydrogen content remains below the TSS. It is potentially, however a source for specimen-to-specimen scatter in the final test results. As shown in

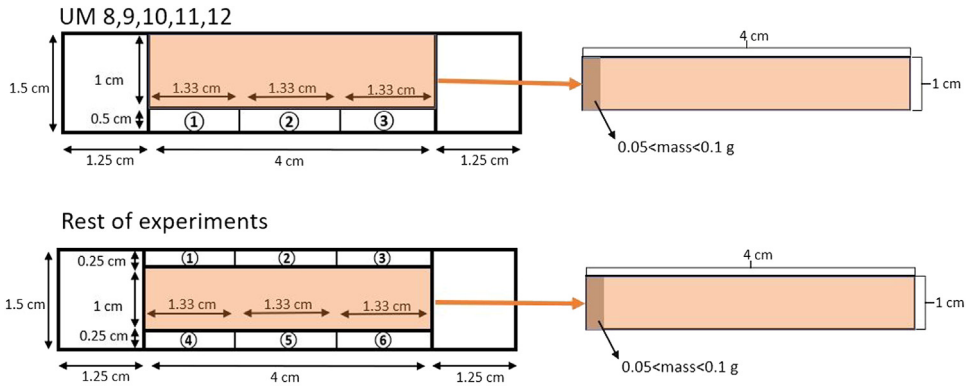

Fig. 2. Sample cutting scheme for initial hydrogen analysis.

Table 1
List of experimental runs conducted in this study.

Specimen	UM8	UM9	UM10	UM11	UM12	UM13	UM14	UM15	UM16	UM17
Temperature (Cold end) [K]	681	695	678	689	687	701	717	723	739	659
Temperature (Hot end) [K]	816	799	814	806	808	794	844	850	865	769
Temperature gradient [K/cm]	34	26	34	29	30	23	32	32	31	27
Initial hydrogen content [wt.ppm]	141	114	203	107	132	194	184	212	169	137
Average hydrogen content after experiment [wt.ppm]	212	274	276	160	132	214	241	280	264	141
Annealing time [days]	27	27	27	26	26	27	22	21	20	34
Sample length [cm]	4	4	4	4	4	4	4	4	4	4
Nickel coating on the sample surface	No	No	No	No	No	No	No	No	No	No
Chamber environment during anneal	Air	Ar gas	Air	Air	Air	Air	Air	Air	Air	Air

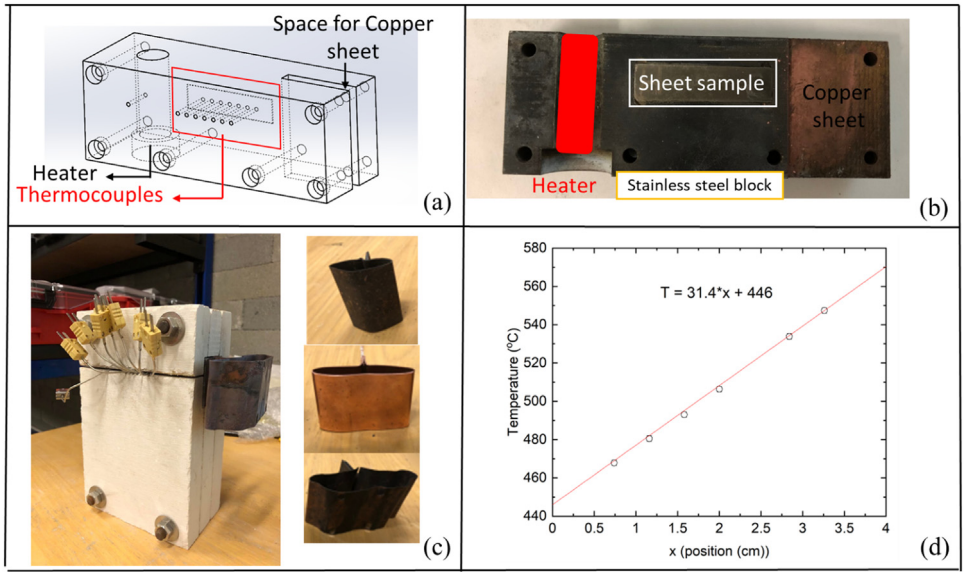

Fig. 3. The annealing facility design. (a) Schematic of the full experimental apparatus facility (b) Pictures of stainless steel block holder (c) Pictures of the insulator and various sizes of copper sheets, (d) Linear temperature profiles of UM15 obtained from thermocouples.

Section 3 (results), although the second condition was not always obeyed, it was consistently possible to eliminate the hydride precipitation from the calculations.

The annealing facility consists of a stainless-steel holder, a heater, eight K-type thermocouples, thermal insulation, a sample chamber, and an electrical box. Fig. 3(a) and (b) show the stainless-steel holder, where the hydrided Zirclaoy-4 sheet sample, heaters, and a copper sheet were arranged. The heater is connected on one side of the stainless-steel holder and the other side was attached to various sizes of copper sheets for the control of temperature distribution and gradient along the sample, as shown in Fig. 3(c). Seven evenly distributed thermocouples are attached to the sample centerline. A linear and high-temperature gradient was achieved with the annealing facility, demonstrated in Fig. 3(d).

2.4. Measuring the hydrogen distribution in the Zircaloy-4 sheet sample after annealing

After hydrogen redistribution, samples were cut into equal pieces along the width direction, as shown in Fig. 4. The hydrogen content of the cut pieces was determined by hot vacuum extraction using the NRC Model 917 performed by Luvak Co. The hydrogen gas was extracted from the specimen in the known volume container at 1200 °C then the pressure of hydrogen gas was

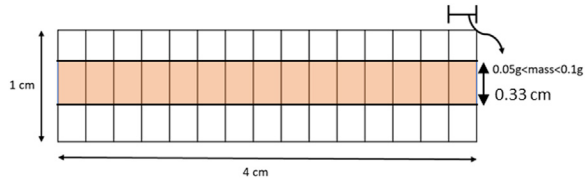

Fig. 4. Sample cutting scheme to determine the hydrogen content after redistribution experiments.

measured to calculate the hydrogen concentration in the specimen. The hydrogen concentration of each section is plotted in a graph, as shown in Fig. 5(a). The error bars in Fig. 5(a) originate from the experimental uncertainty of the hot vacuum extraction determination of the hydrogen concentration.

In each experiment, the determination of the hydrogen concentration slope in log concentration vs 1/T space allows the determination of the heat of transport Q^*. Eqs. (3-5) show how to calculate the slope which determines the heat of transport (Q^*) values:

$$C(x) = C_o \exp\left(\frac{Q^*}{RT(x)}\right) \tag{3}$$

$$\ln C(x) - \ln C_o = \left(\frac{Q^*}{RT(x)}\right) \tag{4}$$

$$\frac{Q^*}{R} = [\ln C(x) - \ln C_o]T(x) = slope \tag{5}$$

where $T(x)$ is the spatial temperature distribution, $C(x)$ is the hydrogen concentration in solid solution at a steady state, C_o is a constant, Q^* is the heat of transport, and R is the gas constant.

Following this derivation, Fig. 5 (b) shows a linear least-squares fitting of a plot of the logarithm of the hydrogen concentration versus the inverse temperature as per Eq. (4). The slope multiplied by the gas constant is the heat of transport (Q^*), as per Eq. (5).

To account for experimental uncertainty, we incorporate the data into a linear regression to find the slope. The distribution of slopes was analyzed to calculate the average value of Q^* and its standard deviation in each experiment. A random point within the error bar is generated at each temperature and the slope is calculated with those points. For each experiment 100,000 datasets were created, which produced a histogram of the calculated slopes. In each of the results presented below, this distribution of results is calculated in each case. From this method, the slope was determined as the average value and the standard derivation was taken as the error bar.

3. Results

3.1. Hydrogen diffusion under a linear temperature gradient

The experimental results are now shown in sequence. The points in Fig. 5(a) show the hydrogen contents measured after experiments UM11 and UM12 as a function of distance (and thus temperature) on the sample. Because it is important to ascertain what portion of the hydrogen is in solid solution, the terminal solid solubility (wt.ppm) of hydrogen in Zircaloy-4 given in Eq. (6) [12]

$$TSS_d = 106,446 \times exp(-4328/T) \tag{6}$$

is also plotted in blue for the temperatures established during the experiment. Also plotted in Fig. 5(a) (in green) is the average hydrogen content in each case (labeled initial Avg H). Once the hydrogen distribution reaches a steady state, the maximum hydrogen content is achieved at the coldest point.

Fig. 5(b) shows the logarithm of the hydrogen content versus the inverse of temperature. The hydrogen, which was initially uni-

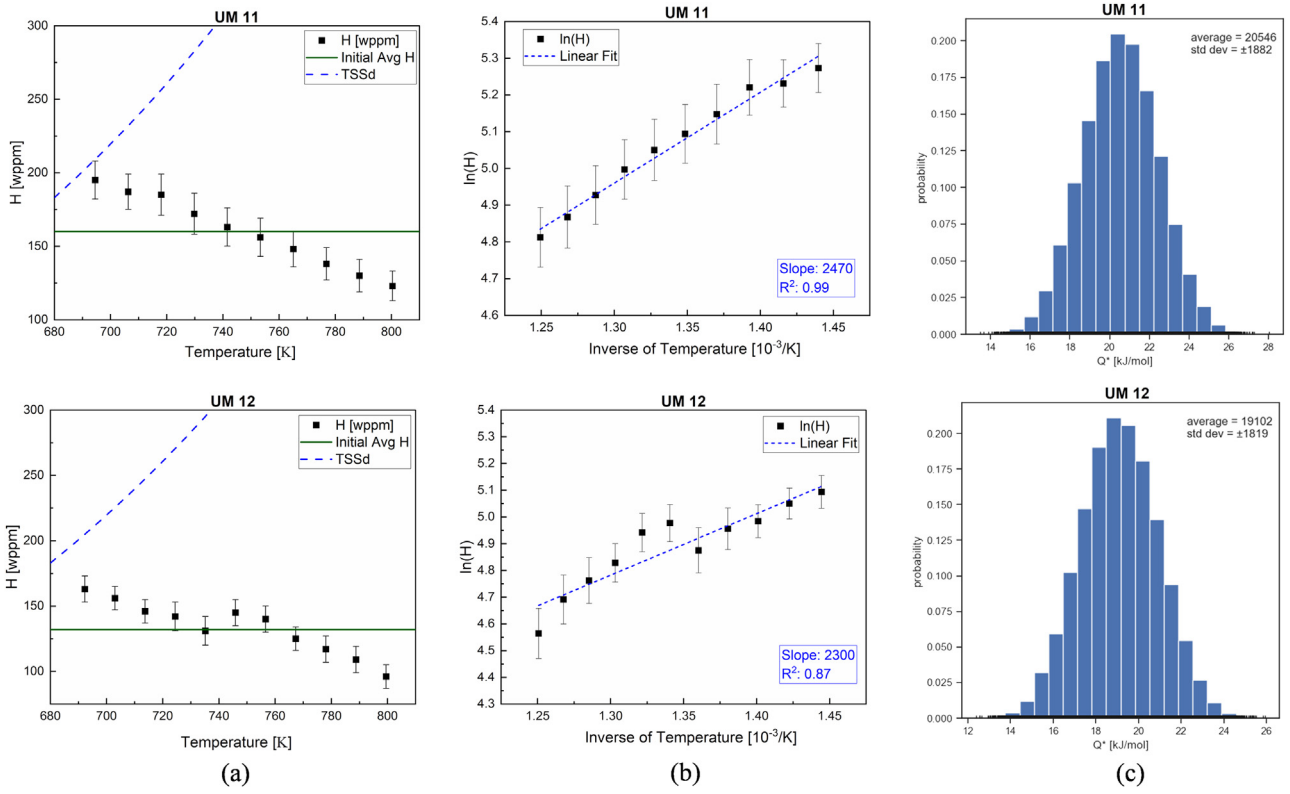

Fig. 5. (a) Hydrogen concentration versus position, (b) Logarithm of the hydrogen concentration versus 1/T graph, (c) Histogram of calculated linear regression slope for 100,000 datasets (see Section 2.4) of UM11 and 12.

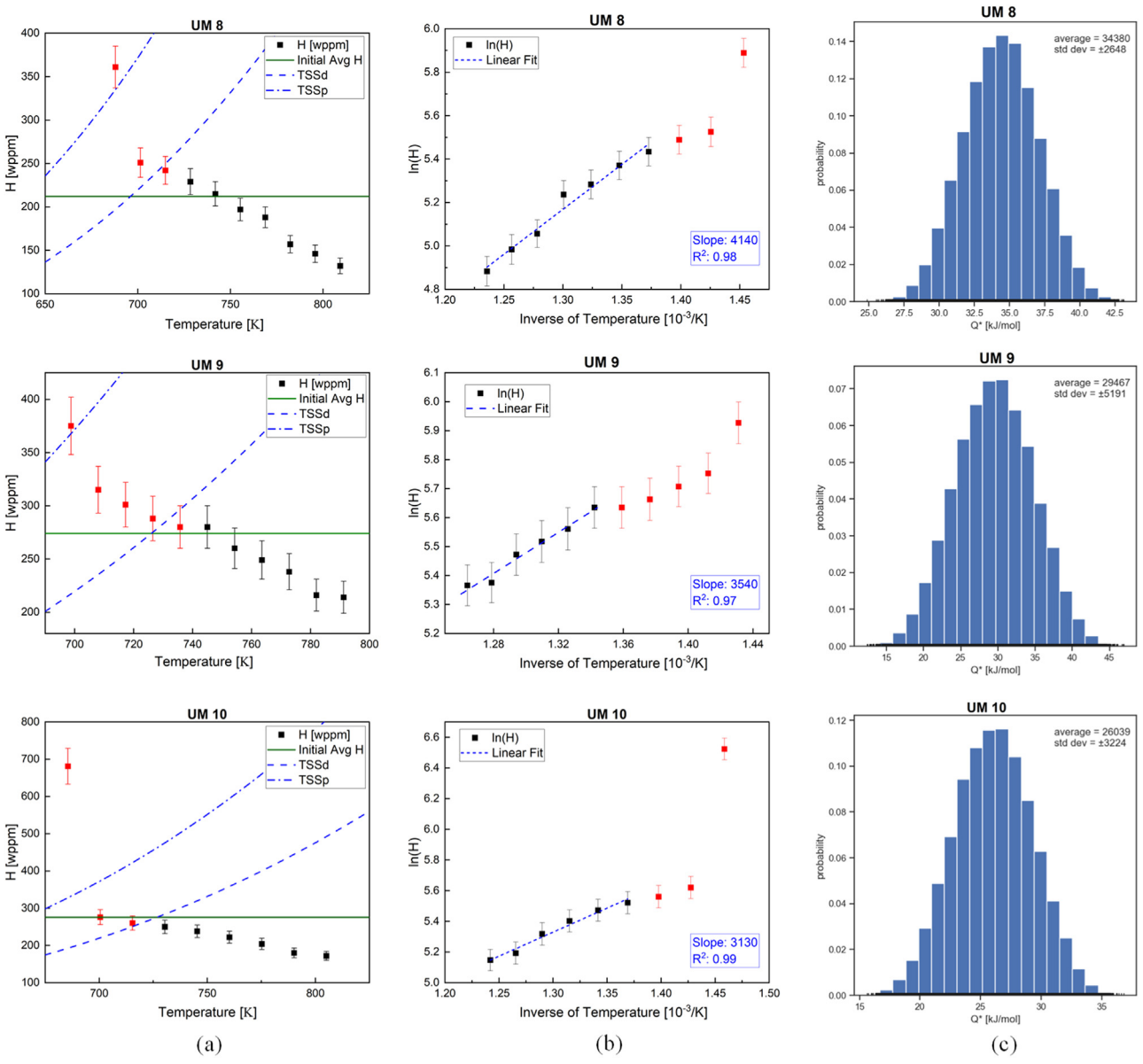

Fig. 6. (a) Hydrogen concentration versus position, (b) Logarithm of the hydrogen concentration versus 1/T, (c) Histogram of calculated linear regression slope for 100,000 datasets (see Section 2.4) of UM8, 9, and 10.

formly distributed, has moved preferentially to the colder side of the sample. The hydrogen contents increase exponentially with decreasing temperature, as per Eq. (3). The figure shows the slope and the R squared value calculated from linear regression. To apply Eq. (5) to calculate Q^*, the hydrogen needs to be in solid solution. It is clear that for the experiments shown in Fig. 5 (UM11 and 12) the points all fall under the TSS_d, so that the hydrides were fully dissolved and all hydrogen was indeed in solid solution during the experiment. Thus, in those cases, all the points were included to calculate Q^* because all points were under TSS_d.

To account for the possible errors in the fit, and as explained in the previous section, an uncertainty analysis was performed using monte carlo techniques to generate slopes 100,000 times. The results are shown in Fig. 5(c). For each case, the average value was taken as Q^* and the standard deviation as the error. For these two cases, the values of Q^* were 20.55 kJ/mol and 19.10 kJ/mol, respectively, which agree well with the linear regression determined best fit slopes through the data shown in Fig. 5(b).

Figs. 6 and 7 are plotted in a similar manner. Fig. 6 shows the results of experiments UM8, 9, and 10. In contrast with the experiments shown in Fig. 5, in each of these cases, the hydrogen content at the cold end was above the TSS, which means that hydrides were precipitated at the colder side. It is clear from Fig. 6 that in some locations the TSSd curve falls below the green curve indicating that hydride precipitation is favored. Precipitation will be even more favored when hydrogen migrates to the cold end during the experiment. Additionally, although the initial hydrogen concentration was aimed to be below TSS, additional hydrogen ingress during the experiment pushed the cold end hydrogen content above it. As a result, the TSSp is reached and hydrides can precipitate. An examination of the plot of logarithm concentration versus distance shows a clear peak on the cold side, indicating precipitation has occurred. Accordingly, those points are colored red and were eliminated from the calculation of Q^*. Once those points are eliminated from the fit, it is clear the remaining points fall on a straight line, as described by Eq. 5.

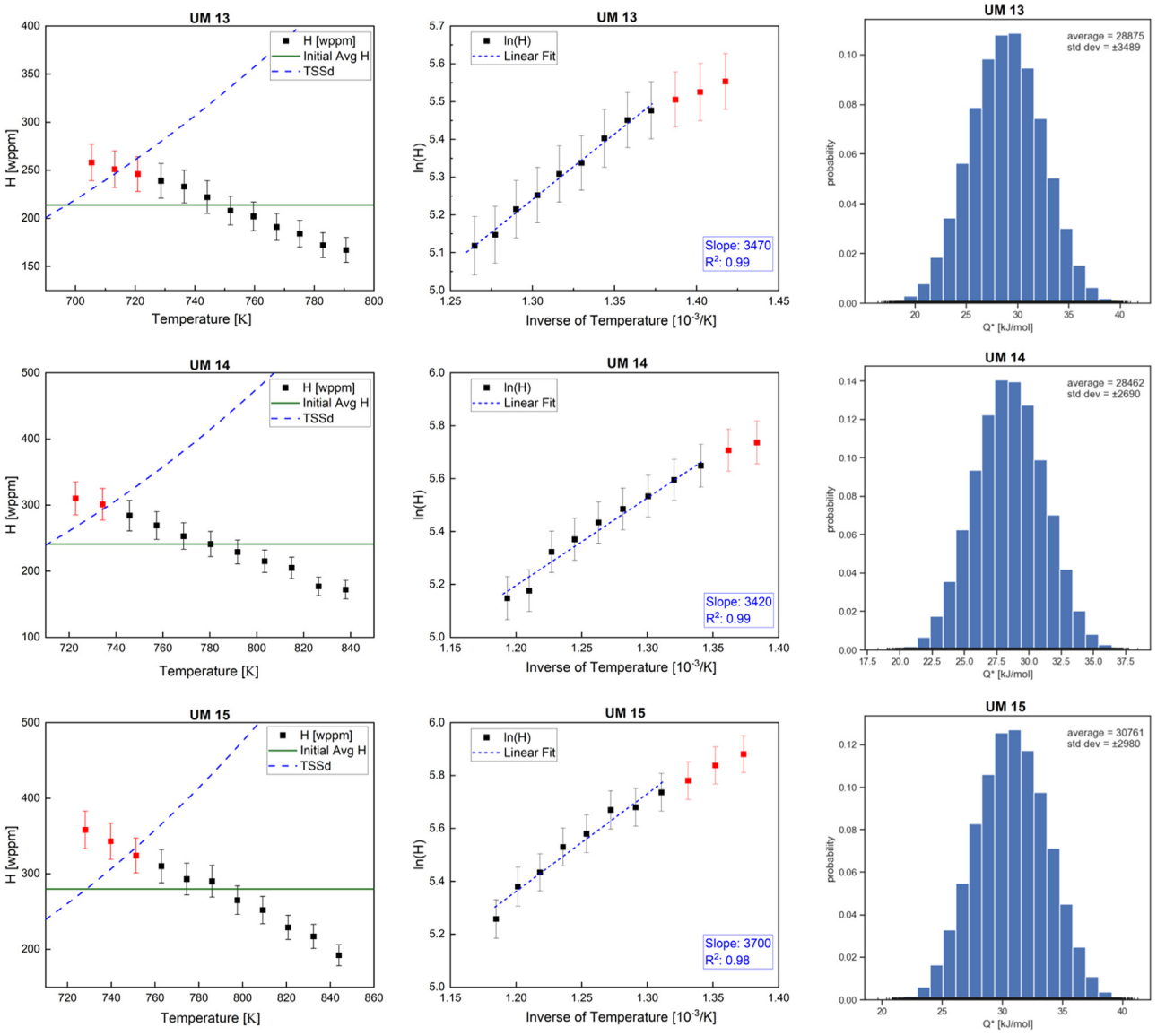

Fig. 7. (a) Hydrogen concentration versus position, (b) logarithm of the hydrogen concentration versus 1/T graph (c) Histogram of calculated linear regression slope for 100,000 datasets (see Section 2.4) of UM13, 14, 15, 16, and 17.

Fig. 7 shows the final hydrogen concentrations measured in experiments UM13,14,15,16, and 17. In these experiments, although the final hydrogen concentration exceeded TSS_D in the colder end, TSSp was not exceeded. Accordingly, no clear increase in hydrogen concentration indicating hydride precipitation was observed. In each case, the initial uniform average hydrogen concentration was below TSS_D even at the coldest spot (TSS_D curve is always above the green curve), so that initially the hydrides are fully dissolved and all the hydrogen is in solid solution. Although TSSp was not reached, after the experiments, the hydrogen concentration at the colder side has increased so that it is likely in the hysteresis region (i.e. between TSSd and TSSp). In that case, if hydrides are not present, the hydrogen remains in solid solution [5]. As a result, no hydrogen concentration peaks are observed. As in the previous case, the points below TSS fall on a straight line, as shown in Fig. 7(b).

4. Discussion

Using the average values of the slope in each case a value of Q^* was calculated from each test specimen using Eq. (5) and is shown in Table 3. These data need to be compared to previously existing data in the literature. For this purpose, two previous experiments which measured Q^* are used to augment the data in this work.

Several experiments performed by Sawatzky are used in this work [13]. They follow the same method, with slightly different parameters. Zircaloy-2 samples were uniformly loaded with hydrogen (130 and 60 wt.ppm) and subjected to a fixed temperature gradient (for 34, 41 and 44 days). At the end of this procedure, the sample was sliced up to measure the distribution of hydrogen in the sample.

In the experiments conducted by Kammenzind, Zircaloy-4 samples were uniformly loaded with hydrogen using gas charging and subjected to a temperature gradient [9]. These experiments cover a wide range of hydrogen contents (47 to 468 wt.ppm) and temperatures (533 to 700 K on the cold side). The durations were determined to allow the system to reach steady state.

The parameters in each case are summarized in Table 2.

Fig. 8 shows a plot of the heat of transport values versus the cold side temperature for the experiments in this study, from Kammenzind's experiments [9] as reviewed by Merlino [10] and Sawatzky [13]. The cold end temperature in Fig. 8 is determined

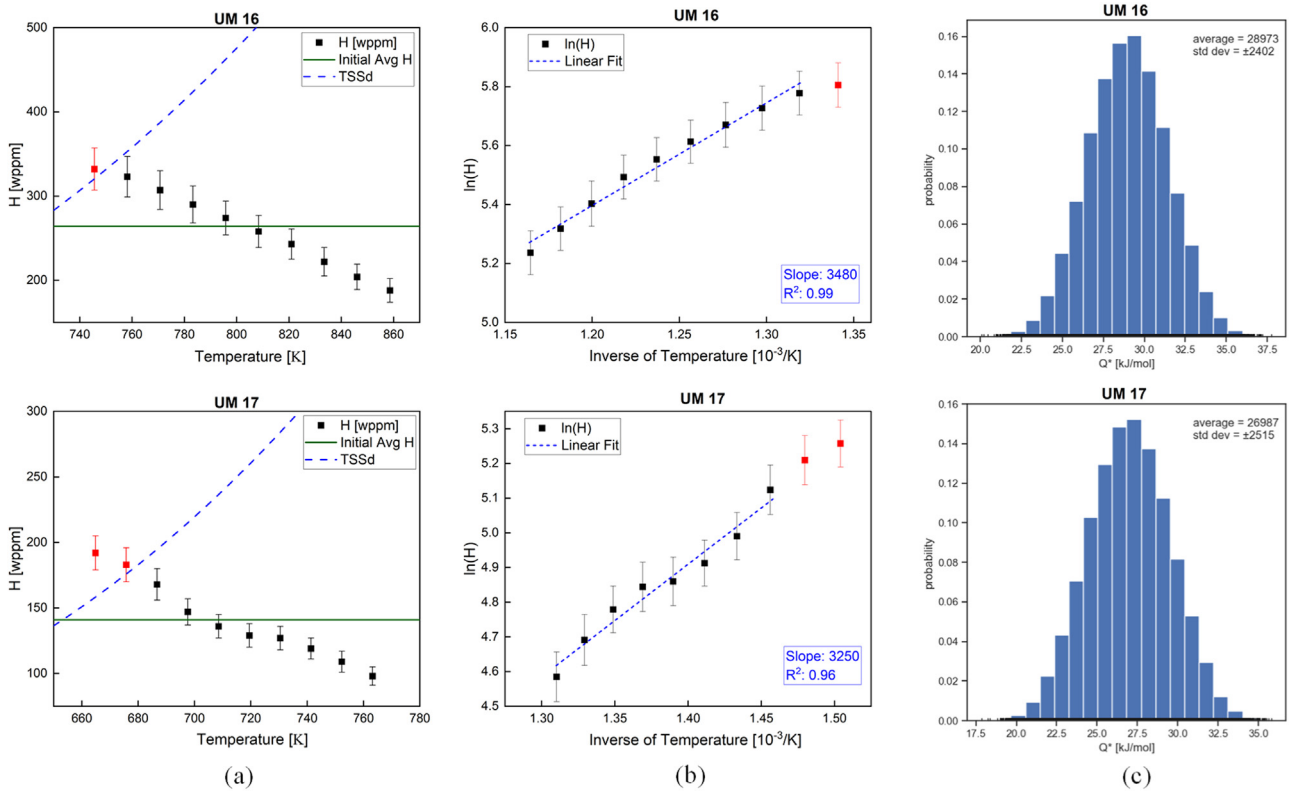

Fig. 7. Continued

Table 2
Sawatzky and Kammenzind experiments.

	Temperature (Cold end) [K]	Temperature (Hot end) [K]	Gradient [K/cm]	Duration [days]	Initial hydrogen contents [wt.ppm]	Calculated Q^* using Eq. (5) [J/mol]	Calculated Q^* using mHNGD (steady-state) [J/mol]
Sawatzky (Zircaloy-2)							
S1	573	773	80	44	60	19665	19665
S2	573	773	80	44	60	25522	25522
S3	403	750	139	34	130	17991	18950*
S4	430	727	119	41	64	15899	17757*
Kammenzind (Zricaloy-4)							
A09a	589	755	66	15	48	28754	30133*
A09b	589	755	66	32	108	33573	33573
A10a	589	755	66	15	64	30053	33629*
A10b	589	755	66	32	62	30873	30873
A11a	644	811	66	9	145	30200	33048*
A11b	644	866	87	20	265	18327	18471*
A12a	644	811	66	9	199	30650	35156*
A12b	644	811	66	18	176	27446	31213*
A13a	702	894	77	6	372	21775	24682*
A14	702	894	77	6	261	20737	22156*
A26b	533	755	87	54	47	24295	24295
A31	589	811	87	26	184	26835	27522*
A45	533	700	66	77	85	26204	26204
A46	533	700	66	77	101	28837	28837
A13b	700	922	87	12	392	19699	20566*

* Corresponding to the data points marked with green arrow in Fig. 8.

with the coldest temperature where all the hydrogen was in solid solution rather than actual cold end temperature in experiments. The experiments from the present study were performed above 659 K to check Q^* values at higher cold end temperatures than the experiments from Kammenzind and Sawatzky studies. The sample names that start with "A" are the data from references [9,10], "UM" are from this study, and "S" are from Sawatzky [13].

One factor that was further considered in this analysis was whether all the experiments in Fig. 8 were run long enough to reach a steady state. For that purpose, the mHNGD model was used to simulate these experiments. The mHNGD model [5,11] can simulate the time dependent hydride distribution considering both hydride dissolution and precipitation kinetics. The input parameters of mHNGD were modified with experimental temperature and Q^* values to fit the experimental conditions. The program shows that, as expected, during the experiment the hydrogen profile evolves from a flat, homogeneous distribution to the steady state hydrogen concentration profile resulting from the equilibrium between

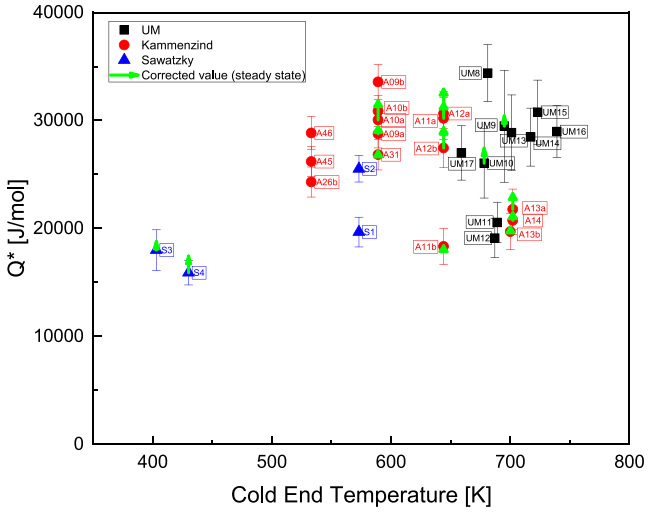

Fig. 8. Heat of transport (Q^*) vs temperature from experiments. Data from Kammenzind [9], Merlino [10], Sawatzky [13] and this study (UM). The sample names that start with "A" are data from references [9,10], "S" are data from Sawatzky [13] and "UM" are data from the experiment in this study. Green arrows show the experiments were non-steady state.

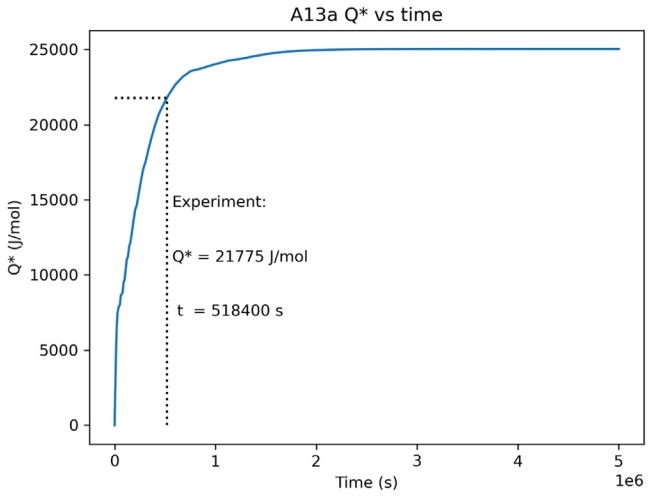

Fig. 9. Heat of transport (Q^*) evolution along the experimental time of A13a using mHNGD [5,11].

Fick and Soret diffusion. Because the slope of the hydrogen profile changes during an experiment until it reaches steady state, an experiment that was interrupted before reaching steady state would produce a slope that does not represent the true Q^* value that would have been obtained at steady state. This check was done for all the experiments in Fig. 8 and it was found that a fraction of those did not reach steady state. These are indicated with green arrows in Fig. 8 and Table 2. The length of the arrows indicates the amount of change. We found that although Q^* undergoes only minor changes in these samples when calculated using steady state values.

Fig. 9 shows an example (from experiment A13a) of how the measured value of Q^* would change from determining it before steady state and at steady state. The dotted line indicates when the experiment was stopped. The steady-state in this study was defined where the hydrogen concentration difference between each time step is less than 1%. In this case, it is clear that the sample did not reach a steady state. The value of Q*, in this case (the largest difference found), changes from 21,775 to 24,682 J/mol.

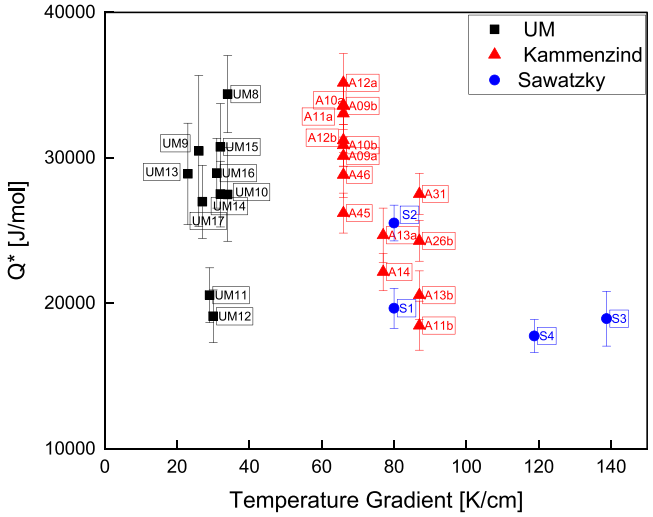

Fig. 10. Heat of transport (Q^*) vs temperature gradient with this study (UM), Kammenzind [9] and Sawatzky [13].

The green arrows in Fig. 8 indicate experiments that did not reach steady-state based on the mHNGD model. Further simulations were performed to find the Q^* values needed to produce those values measured for these experiments that did not reach steady state. Tables 2 and 3 show the corrected Q^* values based on simulation.

What is clear from Fig. 8 is that the value of Q^* is spread on a wide range between roughly 20,000 and 35,000 J/mole. No clear dependence on the cold end temperature is observed. The simple observation of Fig. 8 begs the question: would there be another variable that would allow us to collapse the data? It is clear that even within one set of experiments (such as those conducted in this work or those conducted by Kammenzind and co-workers) the value of Q^* varies widely in the range above, with no obvious dependence on temperature. The experiments in this work and in Kammenzind work were done on Zircaloy-4 whereas those of Sawatzky were done on Zircaloy-2. Although the latter appears on the lower end of the spectrum, only a small number of experiments are available. Attempts to collapse the data by time of anneal, hot end temperature, or hydrogen content were equally unsuccessful.

As discussed earlier in Section 2.3, there is evidence that some of the samples picked up hydrogen during tests. This was also true for some of the Kammenzind specimens, in particular specimens A31, A11b, A13a and A13b. While there is no apparent correlation in Fig. 8 for the specimens experiencing the most pickup to be separated from those experiencing the least, the effect of the pickup on the final distribution is difficult to analyze, not knowing when and the rate at which it happened. Perhaps this may be one factor in the specimen-to-specimen data scatter. Regardless, the preponderance of the data appears to lie between 25,000 J/mol and 35,000 J/mol, with no obvious dependence on test temperature.

We include one more plot, which shows the value of Q^* in the different experiments against the temperature gradient imposed on the sample, as shown in Fig. 10. As specified in Tables 2 and 3., whereas the experiments marked "UM" were conducted using a temperature gradient of ≈20-40 K/cm, Kammenzind and Sawatzky used temperature gradients between 60 and 85 K/cm and Sawatzky's were somewhat higher than that. With the exception of UM11 and UM12, there appears to be an overall trend of decreasing Q^* with increasing temperature gradient. Of course, since each set of experiments had their own temperature gradi-

Table 3
The present experiments.

	Temperature (Cold end) [K]	Temperature (Hot end) [K]	Gradient [K/cm]	Duration [days]	Initial hydrogen contents [wt.ppm]	Calculated Q^* using Eq. (5) [J/mol]	Calculated Q^* using mHNGD (steady-state) [J/mol]
UM8	681	816	34	27	212	34380	34380
UM9	695	799	26	27	274	29467	30470*
UM10	678	814	34	27	276	26039	27485*
UM11	689	806	29	26	160	20546	20560
UM12	687	808	30	26	134	19102	19110
UM13	701	794	23	27	214	28875	28900
UM14	717	844	32	22	241	28462	27510
UM15	723	850	32	21	280	30761	30750
UM16	739	865	31	20	264	28973	28950
UM17	659	769	27	34	141	26987	26980

* Corresponding to the data points marked with green arrow in Fig. 8.

ent, it is possible that another unknown factor particular to each experiment is determinant in Q^*.

5. Conclusion

In this study, Zircaloy-4 sheet samples were uniformly hydrided and annealed under a linear temperature gradient for a long anneal, intended to provide enough time to reach steady-state and to provide significant migration of hydrogen by the Soret effect. The experiment was carefully optimized to yield stable temperature distribution and reliable results. The uncertainties were also evaluated by computer simulation. The experiment was run at a range of temperatures and the resulting hydrogen distribution was measured by successive sample cutting and hot vacuum extraction. The fit of the hydrogen profile allowed to determine the value of the heat of transport of hydrogen in Zircaloy-4, Q^*. The results are as follows:

1 For the range of cold end temperatures between 659 K and 739 K, the value of Q^* was 20-35 kJ/mol.
2 The Q^* results roughly agree with Kammenzind experiments conducted over a cold end temperature between 533 K and 700 K.
3 Q^* values of some experiments in the Kammenzind data set were concluded with BISON simulations to have not reached steady state values and were therefore underestimated. They were corrected using the mHNGD model in BISON.
4 Some of the test specimens in the data set reported herein apparently picked up hydrogen during test, which introduces one source of uncertainty that is difficult to evaluate. This is also true of the Kammenzind data set. While one might expect hydrogen pick-up during test to lead to a non-steady state profile leading to low inferred Q^* values, there is no apparent correlation in the range of measured Q^* values with specimens experiencing the most hydrogen pickup during test.
5 The preponderance of the data from this work and the Kammenzind work fall in the range of 25,000 J/mol to 35,000 J/mol, with no trend with test temperature. This suggests the value used in the BISON model may be low and a more appropriate value might be 30,000 J/mol.

Declaration of Competing Interest

The authors declare that they have no known competing financial interests or personal relationships that could have appeared to influence the work reported in this paper.

CRediT authorship contribution statement

Soyoung Kang: Conceptualization, Validation, Formal analysis, Investigation, Writing – original draft, Visualization. **Pei-Hsun Huang:** Validation, Conceptualization, Investigation, Writing – original draft, Visualization. **Victor Petrov:** Supervision, Conceptualization, Validation, Writing – review & editing. **Annalisa Manera:** Supervision, Conceptualization, Validation, Writing – review & editing. **Taehwan Ahn:** Supervision, Conceptualization, Validation, Writing – review & editing. **Bruce Kammenzind:** Supervision, Validation, Conceptualization, Resources, Writing – review & editing. **Arthur T. Motta:** Supervision, Conceptualization, Validation, Writing – review & editing, Funding acquisition.

Data Availability

Data will be made available on request.

Acknowledgments

This work was performed with the support of the DOE NEUP IRP-17-13708 project “Development of a Mechanistic Hydride Behavior Model for Spent Fuel Cladding Storage and Transportation”; we acknowledge helpful discussions with the other members of the IRP project.

References

[1] C. Lemaignan, A.T. Motta, Zirconium alloys in nuclear applications, Mater. Sci. Technol. (2006) Wiley-VCH Verlag GmbH & Co. KGaA, doi:10.1002/9783527603978.mst0111.
[2] A.T. Motta, L. Capolungo, L.Q. Chen, M.N. Cinbiz, M.R. Daymond, D.A. Koss, E. Lacroix, G. Pastore, P.C.A. Simon, M.R. Tonks, B.D. Wirth, M.A. Zikry, Hydrogen in zirconium alloys: a review, J. Nucl. Mater. 518 (2019) 440–460, doi:10.1016/J.JNUCMAT.2019.02.042.
[3] E. Hillner, Hydrogen absorption in Zircaloy during aqueous corrosion, effect of environment, United States, AEC Res. Dev. (1964) WAPD-TM-411 https://www.osti.gov/biblio/4646726 .
[4] R.S. Daum, S. Majumdar, D.W. Bates, A.T. Motta, D.A. Koss, M.C. Billone, in: On the Embrittlement of Zircaloy-4 Under RIA-Relevant Conditions,: Thirteenth International Symposium on Zirconium in the Nuclear Industry, ASTM STP 1423, 2002, pp. 702–718, doi:10.1520/stp11412s.
[5] E. Lacroix, P.-C. Simon, A. Motta, J. Almer, in: Zirconium Hydride Precipitation and Dissolution Kinetics in Zirconium Alloys, Zirconium in the Nuclear Industry: 19th International Symposium, STP 1622, 2021, pp. 67–91, doi:10.1520/STP162220190035.
[6] O. Courty, A.T. Motta, J.D. Hales, Modeling and simulation of hydrogen behavior in Zircaloy-4 fuel cladding, J. Nucl. Mater. 452 (2014) 311–320, doi:10.1016/j.jnucmat.2014.05.013.
[7] K.G. Denbigh, H.B. Callen, K.G. Denbigh, H.B. Callen, The Thermodynamics of the steady state, AmJPh 20 (1952) 385 –385, doi:10.1119/1.1933259.
[8] M. Puls, The Effect of Hydrogen and Hydrides on The Integrity of Zirconium Alloy Components: Delayed Hydride Cracking, Springer-Verlag, London, 2012.
[9] B. Kammenzind, D. Franklin, H. Peters, W. Duffin, Hydrogen pickup and redistribution in alpha-annealed Zircaloy-4, ASTM Spec, Tech. Publ. 1295 (1996) 338–370, doi:10.1520/STP16180S.

[10] J.T. Merlino, Master of Engineering Paper in Nuclear Engineering, The Pennsylvania State University, 2019.
[11] F. Passelaigue, P.-C.A. Simon, A.T. Motta, Predicting the hydride rim by improving the solubility limits in the Hydride Nucleation-Growth-Dissolution (HNGD) model, J. Nucl. Mater. 558 (2022) 153363, doi:10.1016/J.JNUCMAT.2021.153363.
[12] A. McMinn, E. Darby, J. Schofield, The terminal solid solubility of hydrogen in zirconium alloys, ASTM Spec. Tech. Publ. 1354 (2000) 173–195, doi:10.1520/STP14300S.
[13] A. Sawatzky, Hydrogen in zircaloy-2: Its distribution and heat of transport, J. Nucl. Mater. 2 (1960) 321–328, doi:10.1016/0022-3115(60)90004-0.